Ultrasound in Med. & Biol., Vol. 45, No. 6, pp. 1407–1416, 2019

0301-5629/$ - see front matter

https://doi.org/10.1016/j.ultrasmedbio.2019.02.008

● *Original Contribution*

PROSPECTIVE EVALUATION OF HEPATIC STEATOSIS USING ULTRASOUND ATTENUATION IMAGING IN PATIENTS WITH CHRONIC LIVER DISEASE WITH MAGNETIC RESONANCE IMAGING PROTON DENSITY FAT FRACTION AS THE REFERENCE STANDARD

Sun Kyung Jeon,* Jeong Min Lee,*,†,‡ Ijin Joo,*,† Jeong Hee Yoon,*,† Dong Ho Lee,*,† Jae Young Lee,*,†,‡ and Joon Koo Han*,†,‡

* Department of Radiology, Seoul National University Hospital, Seoul, South Korea; † Seoul National University College of Medicine, Seoul, South Korea; and ‡ Institute of Radiation Medicine, Seoul National University Medical Research Center, Seoul, South Korea

(*Received* 26 *October* 2018; *revised* 31 *January* 2019; *in final from* 6 *February* 2019)

Abstract—The purpose of our study was to investigate the diagnostic performance of 2-D ultrasound attenuation imaging (ATI) for the assessment of hepatic steatosis in patients with chronic liver disease using magnetic resonance imaging proton density fat fraction (MRI-PDFF) as the reference standard. We prospectively analyzed 87 patients with chronic liver disease who had reliable measurements at both ATI and MRI-PDFF. For the detection of hepatic steatosis of MRI-PDFF ≥5% and MRI-PDFF ≥10%, ATI measurements yielded areas under the receiver operating characteristic curve of 0.76 and 0.88, respectively (95% confidence intervals: 0.66–0.85 and 0.79–0.94). Attenuation coefficients at ATI were moderately correlated with MRI-PDFF (ρ = 0.66). In conclusion, attenuation coefficients at ultrasound ATI were well correlated with MRI-PDFF and, thus, may provide good diagnostic performance in the assessment of hepatic steatosis, making these coefficients a promising tool for the non-invasive assessment and quantification of hepatic steatosis. (E-mail: jmsh@snu.ac.kr) © **2019 World Federation for Ultrasound in Medicine & Biology. All rights reserved.**

Key Words: **Hepatic steatosis, Chronic liver disease, Ultrasound, Attenuation imaging, Fat quantification, Proton density fat fraction.**

INTRODUCTION

Hepatic steatosis is one of the most common conditions in chronic liver disease (CLD), with an increasing prevalence ranging between 16% and 45% in Western societies and between 9% and 29% in Eastern societies (Blachier et al. 2013). In addition to patients with non-alcoholic fatty liver disease (NAFLD), hepatic steatosis can also be found in patients with CLDs of other etiologies, including chronic hepatitis C virus (HCV) infections and alcoholic liver disease, as they are themselves steatogenic, and the metabolic syndrome can be superimposed on other liver diseases (Berzigotti 2014). Furthermore, metabolic risk factors such as obesity, hepatic steatosis and diabetes mellitus have been reported to be associated with poor treatment response in HCV infections (Elgouhari et al. 2009; Fabiani et al. 2018; Modaresi Esfeh and Ansari-Gilani 2016) and with increased risk for hepatocellular carcinoma in patients with CLDs (Huang et al. 2018; Yu et al. 2017). Therefore, evaluation of hepatic steatosis and fibrosis is crucial in the management of patients with CLDs (Berzigotti 2014). At present, liver biopsy is the reference standard for hepatic fibrosis and steatosis; however, it is an invasive procedure with inherent risks of peri- and postprocedural complications as well as inter-observer variability (Rockey et al. 2009). Therefore, a reliable, non-invasive, quantitative diagnostic tool for the assessment of hepatic steatosis would be desirable in terms of both risk assessment and monitoring of patients with CLDs.

To date, ultrasonography (US) has been the most common imaging modality used to evaluate hepatic steatosis owing to its availability, low cost and tolerability (Mishra and Younossi 2007; Saadeh et al. 2002). However,

Address correspondence to: Jeong Min Lee, Department of Radiology, Seoul National University Hospital and Seoul National University College of Medicine, 101 Daehangno, Jongno-gu, Seoul, 03080, Korea. E-mail: jmsh@snu.ac.kr

a previous report suggested that it may underestimate the prevalence of hepatic steatosis in the presence of <20% fat (Dasarathy et al. 2009). On the other hand, multi-echo Dixon methods and magnetic resonance spectroscopy, which measure the magnetic resonance imaging proton density fat fraction (MRI-PDFF), have been proven to correlate well with histology-based steatosis grades and, thus, have emerged as leading non-invasive modalities for steatosis quantification (EASL-EASD-EASO 2016; Idilman et al. 2013; Permutt et al. 2012; Reeder et al. 2011; Tang et al. 2013). Yet, despite its strengths, magnetic resonance imaging (MRI) remains expensive and may not be routinely accessible at many geographic locations, thereby limiting its use in clinical practice.

Recently, ultrasound-based attenuation techniques such as the controlled attenuation parameter (CAP) and 2-D attenuation imaging (ATI), which measures the attenuation coefficient (dB/cm/MHz) of ultrasound signals, have been developed as novel techniques for the assessment of hepatic steatosis (Chon et al. 2014; Fujii et al. 2002; Fujiwara et al. 2018; Lee et al. 2017b; Lin et al. 1988; Sasso et al. 2012). Two-dimensional ATI, in particular, can also provide additional advantages of simultaneous acquisition of gray-scale diagnostic images and a larger sample volume compared with CAP (Sasso et al. 2010), potentially allowing rapid, non-invasive, bedside assessment of hepatic steatosis, which would be more accessible than MRI (Han et al. 2018; Runge et al. 2018; Sasso et al. 2010). To the best of our knowledge, however, no studies have investigated the diagnostic performance of ATI in the evaluation of hepatic steatosis in patients with CLDs.

Therefore, the purpose of this prospective study was to investigate the diagnostic performance of ATI for the assessment of hepatic steatosis using MRI-PDFF as the reference standard.

METHODS

Patients

This prospective study was approved by our institutional review board, and written informed consent was obtained from all patients. Between January 2018 and July 2018, 92 patients (68 men and 24 women; age, mean ± standard deviation: 65.1 ± 10.2 y; range: 33−86 y) who met the eligibility criteria and gave written informed consent were included in this study. Included in this study were (i) patients with CLD or liver cirrhosis who were referred to our radiology department for US evaluation of the cause of liver function test abnormalities or for surveillance of hepatocellular carcinoma, and (ii) patients who had undergone MRI-PDFF and magnetic resonance elastography (MRE) within the 3 mo before the US examination.

The median interval between MRI-PDFF and ATI was 21.5 d (range: 0−76 d). Presence of type 2 diabetes, body mass index (BMI), etiology of chronic liver disease and laboratory data including alanine aminotransferase (ALT) and aspartate aminotransferase (AST) levels on the day of the ATI examination were recorded.

2-D ultrasound attenuation imaging

All patients underwent conventional gray-scale ultrasound and ATI performed by one operator (J.M.L. with 26 y of experience in abdominal ultrasound) who was blinded to the patients' clinical details as well as MRI-PDFF and MRE results. US and ATI examinations were performed using a diagnostic ultrasound system (Aplio i800, Canon Medical Systems, Tochigi, Japan) with a 1- to 8-MHz convex probe in patients who had fasted for at least 6 h. All images were obtained in the supine position and in the intercostal planes.

During the gray-scale US examinations, the operator evaluated and categorized the degree of hepatic steatosis into four groups (S0 = no steatosis, S1 = mild steatosis, S2 = moderate steatosis and S3 = severe steatosis) according to Hamaguchi's ultrasonographic scoring system, which is based on the following US features: increased echogenicity of the liver parenchyma, altered hepatorenal contrast, deep attenuation and blurred blood vessels (Hamaguchi et al. 2007).

For ATI examinations, two sessions of attenuation coefficient measurements were performed on the same day with each person, with each session including 10 consecutive attenuation coefficient measurements. For attenuation coefficient measurement, an approximately 4 × 8-cm sample box was positioned in the right lobe of the liver *via* an intercostal approach during several seconds of breathholding. The degree of attenuation was color-coded and displayed in the sampling box of ATI. There are three major mechanisms of attenuation when ultrasound passes through a depth: (i) absorption by conversion of sound energy into heat, (ii) reflection by removal of sound energy from its re-direction of some sound back to transducer and (iii) scattering by removal of sound energy from its re-direction in various directions. So, we tried to acquire ATI color maps as uniform as possible. There are two factors that affect attenuation in ultrasound waves: (i) the media through which ultrasound travels, and (ii) the frequency at which the ultrasound is transmitted through the media. If the transmitting frequency is fixed, the attenuation depends on the medium. This means that the same media have the same attenuation in the same depth range. So, the system receives the returning echo signal and eliminates the focus-dependent beam profile and compensated

gain profile from the original receiving signal. Then, the system calculates adjusted echo intensity and estimates the attenuation coefficient as

$$\alpha = -\frac{1}{2f}\frac{dI_c}{dz}$$

where α = attenuation coefficient (dB/cm/M), I_c = adjusted intensity (dB), f = central frequency (MHz) and z = depth (cm).

Non-homogeneous areas such as large vessels and cystic structures were automatically excluded from the ATI map by using the structure removal filtering system internally and were presented as vacancies. By careful avoidance of large vessels and areas of reverberation artifacts, a 3 × 3-cm region of interest (ROI) for measurement was set within the sampling box of ATI (Fig. 1). Then, the average attenuation coefficient result was displayed in units of dB/cm/MHz. The coefficient of determination was also displayed as an R^2 value along with the attenuation coefficient at each acquisition, allowing the operator to confirm the optimal location for ROI placement to improve accuracy. The R^2 values were classified as poor ($R^2 < 0.80$), good ($R^2 = 0.80–0.89$) or excellent ($R^2 \geq 0.90$). Only the attenuation coefficient with $R^2 \geq 0.80$ was considered to be a valid acquisition, and technical success was defined as a success rate (computed as the number of valid acquisitions divided by the total number of acquisitions) ≥60%. Reliable measurements were defined as an interquartile range ([IQR] the difference between the 75th and 25th percentiles) less than 30% of the median value (Ferraioli et al. 2015).

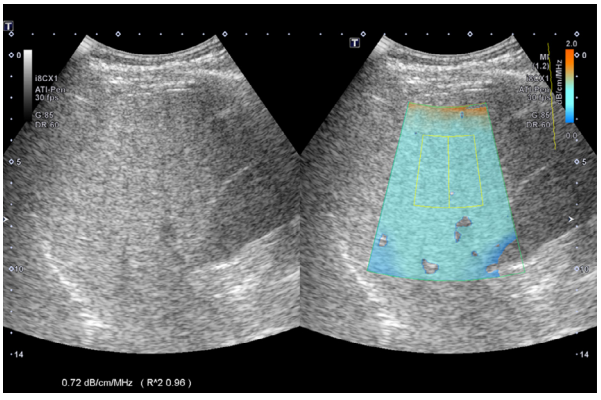

Fig. 1. Two-dimensional ultrasound attenuation imaging. During the attenuation imaging examination, a B-mode ultrasound image (left) and a color-coded attenuation map (right) are provided simultaneously. Areas of significant errors in attenuation calculation, such as large vessels and areas with reverberation artifacts, are excluded on the attenuation map and are presented as vacancies. The attenuation coefficient and the coefficient of determination (R^2 value) are displayed in each acquisition.

MRI-PDFF and MR elastography

At our institution, MRI-PDFF and MRE are incorporated into the routine liver MRI protocol to assess hepatic steatosis and fibrosis in patients with chronic liver diseases. In this study, all patients underwent chemical shift 3-D spoiled gradient-recalled echo sequences for PDFF measurements and MRE examinations using one of the 3.0-T magnetic resonance (MR) systems at our institution: Ingenia 3.0-T (Philips Medical System, Best, Netherlands: n = 54); Skyra 3.0-T (Siemens Healthineers, Erlangen, Germany: n = 29); and Discovery MR 750w 3.0-T (GE Medical Systems, Milwaukee, WI, USA: n = 9). PDFF is defined as the ratio of MR imaging-visible fat protons to the sum of MR imaging-visible fat and bulk (free) water protons (Yokoo et al. 2018). In this study, we used complex-based chemical shift-encoded water-fat reconstruction techniques for MRI PDFF measurements that were provided by the MR vendors. All of the MRI-PDFF sequences used six echoes, T2* correction calculated from signal decay, a low flip angle to minimize the T1 bias between fat and water and a multipeak fat model (Reeder et al. 2009). PDFF maps were generated from corrected water and fat images as fat signal intensities/(fat signal intensities + water signal intensities) (Yokoo et al. 2018). PDFF and T2* maps were automatically generated by each vendor's algorithm, and the PDFF map was used for measurement.

One radiologist (S.K.J., with 5 y of experience in liver MRI) who was blinded to the ATI measurement results manually placed circular ROIs in each of the nine Couinaud liver segments on the MRI-PDFF map of each patient. Each ROI with a diameter of 1 cm was placed near the center of each segment, while taking care to avoid major vessels, the liver edge and artifacts. The PDFF in each of the nine ROIs was recorded, and the PDFF value across the entire liver was reported as the mean of the PDFF values of all nine ROIs (Tang et al. 2013). No images had substantial artifacts that disrupted ROI measurements. Detailed imaging parameters of MRI-PDFF are provided in Appendix A.

On the same day, MRE was also performed in the supine position with 60-Hz vibrations applied to the abdominal wall on the basis of a 2-D gradient echo sequence, and the four sections were acquired in four consecutive breathholds at the end of expiration. MR elastogram maps were automatically generated from the scanner using a direct inversion algorithm (Lee et al. 2017a). Liver stiffness (LS) was measured by one abdominal radiologist (S.K.J.) using a free-draw method, excluding large hepatic vessels, fissures and focal liver lesions (Yoon et al. 2013). LS values (in kPa) of each patient were calculated as the median value of the regions of interest (mean area = 2620.5 ± 132.7 mm^2).

To discriminate between various METAVIR fibrosis stages at MRE, we used recently published meta-analysis cutoff values (Xiao et al. 2017) of 2.99 kPa for significant fibrosis (≥F2), 3.62 kPa for severe fibrosis (≥F3) and 4.63 kPa for liver cirrhosis (F4). Detailed imaging parameters of MR elastography are provided in Appendix B.

Statistical analyses

All patients' demographic data and imaging data were summarized using the mean and standard deviation for continuous variables and numbers and percentages for categorical variables. Correlations between attenuation coefficients at ATI and MRI-PDFF or the visual grade of hepatic steatosis were assessed using the Spearman rank correlation coefficient. Kruskal–Wallis and Mann–Whitney *U*-tests were used to compare the attenuation coefficients obtained at ATI with the different categories of hepatic fat content assessed with MRI-PDFF. Receiver operating characteristic (ROC) curve analyses were used to assess the diagnostic accuracy of attenuation coefficients at ATI for the detection of hepatic steatosis (defined as MRI-PDFF ≥5%) and of hepatic fat content ≥10% steatosis (MRI-PDFF ≥10%) (Caussy et al. 2018). For each ROC analysis, the area under the ROC curve (AUC), optimal thresholds, sensitivity and specificity were calculated. The optimal threshold was determined using the Youden index (Youden 1950). Multivariate linear regression analysis was used to identify significant determinant factors for attenuation coefficients at ATI. To evaluate intra-operator reliability (repeatability), intra-class correlation coefficients (ICCs) and coefficients of variation (CVs) were obtained for comparison of the two ATI sessions. ICCs were reported with a 95% confidence interval (CI) and were classified as poor (ICC = 0.00–0.20), fair to good (ICC = 0.40–0.75) or excellent (ICC >0.75) (Hudson et al. 2013). CVs ≤10%, 10%–25% and ≥25% were considered to indicate good, moderate and poor reproducibility, respectively (Iellamo et al. 1996). All p values <0.05 were considered to indicate a statistically significant difference. All statistical analyses were performed using MedCalc software (Version 16.4.1, Ostend, Belgium).

RESULTS

Eighty seven patients were included for analysis, after excluding 5 patients because of either technical failure (n = 4) or unreliable results (n = 1, IQR/median = 34%) on ATI. Among the 87 patients, the prevalence of hepatic steatosis (MRI-PDFF ≥5%) and hepatic fat content ≥10% (MRI-PDFF ≥10%) was 57.5% (n = 50) and 23.0% (n = 20), respectively. The demographic characteristics of the study patients whose data were analyzed (n = 87) are summarized in Table 1.

Table 1. Baseline characteristics of patients (N = 87)

Age (y)	65.1 ± 10.2
Sex	
Male	64 (73.6)
Female	23 (26.4)
Body mass index (kg/m^2)	25.4 ± 3.6
Type 2 diabetes	16 (18.4)
Skin-to-liver capsular distance (mm)	17.0 ± 4.5
Etiology of liver disease	
Hepatitis B virus-related	69 (79.3)
Hepatitis C virus-related	8 (9.2)
Alcoholism	3 (3.4)
Non-alcoholic fatty liver	3 (3.4)
Cryptogenic	4 (4.6)
Aspartate aminotransferase (U/L)	31.7 ± 12.5
Alanine aminotransferase (U/L)	27.7 ± 13.9
Visual grade of hepatic steatosis	
S0 (no steatosis)	38 (43.7)
S1 (mild)	29 (33.3)
S2 (moderate)	17 (19.5)
S3 (severe)	3 (3.4)
Hepatic steatosis at MRI-PDFF	
MRI-PDFF <5%	37 (42.5)
MRI-PDFF 5%–10%	30 (34.5)
MRI-PDFF ≥10%	20 (23.0)
Liver stiffness at MRE (kPa)	4.1±1.9
Fibrosis grade according to MRE	
F0 or F1	26 (29.9)
F2	14 (16.1)
F3	21 (24.1)
F4	26 (29.9)

MRI-PDFF = magnetic resonance imaging proton-density fat fraction, MRE = magnetic resonance elastography

Data are expressed as the mean ± standard deviation for continuous variables and as the number (percentage) for categorical variables.

Correlation between ATI and visual grade of hepatic steatosis and between ATI and MRI-PDFF

Attenuation coefficients at ATI were found to be well correlated with visual grades of hepatic steatosis (ρ = 0.77, 95% CI: 0.67–0.84, $p < 0.001$). There was a moderate correlation between attenuation coefficients at ATI and MRI-PDFF (ρ = 0.66, 95% CI: 0.52–0.76, $p < 0.001$). In patients who underwent ATI and MRI-PDFF on the same day (n = 12), attenuation coefficients at ATI and MRI-PDFF also were moderately correlated (ρ = 0.6, 95% CI: 0.22–0.83, $p = 0.005$). Attenuation coefficients in patients with MRI-PDFF ≥10% (median: 0.73, range: 0.69–0.82 dB/cm/MHz) were significantly higher than those in patients with MRI-PDFF 5%–10% (0.65, 0.65–0.69 dB/cm/MHz) and MRI-PDFF <5% (0.58, 0.53–0.64 dB/cm/MHz) ($p < 0.001$ and $p < 0.001$, respectively). The distribution of attenuation coefficients at ATI measurements across different categories of hepatic fat content as assessed by MRI-PDFF is illustrated in Figure 2. In patients with a METAVIR fibrosis score ≤F2 (patients without severe hepatic fibrosis, n = 40), attenuation coefficients at ATI and MRI-PDFF exhibited a moderate correlation (ρ = 0.72, 95% CI: 53–0.84, $p < 0.001$), whereas attenuation coefficients at

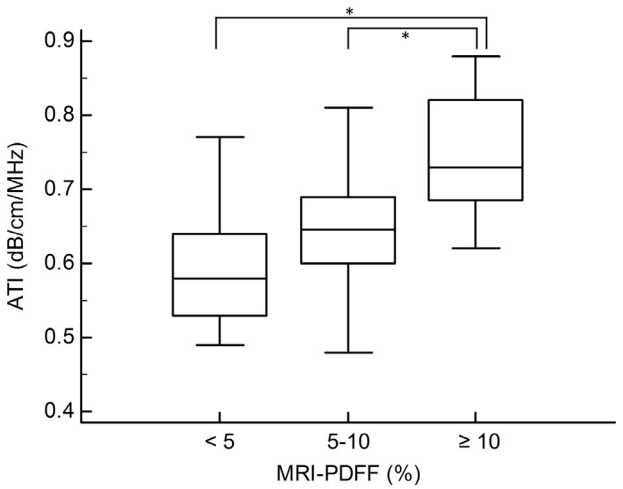

Fig. 2. Distribution of attenuation coefficients at attenuation imaging (ATI) stratified by the hepatic fat content assessed by magnetic resonance imaging proton-density fat fraction (MRI-PDFF). Attenuation coefficients at ATI increase with the grade of hepatic steatosis assessed by MRI-PDFF, with median attenuation coefficients of 0.58, 0.65 and 0.73 dB/cm/MHz, respectively (Kruskal–Wallis test, $p < 0.001$). Asterisks indicates a significant p value between the two groups (Mann–Whitney U-test, $p < 0.001$).

ATI and MRI-PDFF in patients with a fibrosis score of F3 or F4 (patients with severe fibrosis or cirrhosis, n = 47) exhibited a weak correlation (ρ = 0.40, 95% CI: 0.13–0.62, $p = 0.005$).

Diagnostic accuracy of ATI for the detection of hepatic steatosis (MRI-PDFF ≥5%) and hepatic fat content ≥10% (MRI-PDFF 10%)

The AUC of attenuation coefficients at ATI for the detection of hepatic steatosis (MRI-PDFF ≥5%) was 0.76 (95% CI: 0.66–0.85) using a cutoff point of 0.59 dB/cm/MHz. Sensitivity and specificity were 88.0% and 62.2%, respectively. The AUC for the detection of hepatic fat content ≥10% (MRI-PDFF ≥10%) was 0.88 (95% CI: 0.79–0.94) using a cutoff point of 0.65 dB/cm/MHz with 85.0% sensitivity and 71.6% specificity (Table 2, Fig. 3).

Factors affecting the attenuation coefficient at ATI

The attenuation coefficient at ATI significantly increased along with the fat fraction at MRI-PDFF, BMI, skin-to-liver capsular distance, ALT level and liver stiffness at MRE. Conversely, age, sex, presence of type 2 diabetes and AST were not significantly associated with the attenuation coefficient at ATI. Multivariate linear regression analysis revealed that hepatic fat fraction at MRI-PDFF ($p < 0.001$) and stage of hepatic fibrosis ($p = 0.004$) had a significant positive effect on attenuation coefficients at ATI (Table 3). There was a moderate correlation between attenuation coefficient at ATI and MRI-PDFF in patients with skin-to-liver distances <20 mm (n = 72) and <25 mm (n = 81) (ρ = 0.66 and 0.63, 95% CI: 0.51–0.77 and 0.49–0.75, p values < 0.001, respectively). There was no statistically significant correlation in patients with skin-to-liver distances ≥20 mm (n = 15) and ≥25 mm (n = 6) ($p = 0.103$ and $p = 0.327$, respectively). In terms of BMI, there was a moderate correlation between attenuation coefficient at ATI and MRI-PDFF in patients with BMI <25 kg/m^2 (n = 47) and 25 ≤ BMI < 30 kg/m^2 (n = 33) (ρ = 0.70 and 0.65, 95% CI: 0.52–0.82 and 0.39–0.81, p values <0.001, respectively), whereas there was no statistically significant correlation in patients with BMI ≥30 kg/m^2 (n = 7, $p = 0.324$).

Intra-operator reliability (repeatability) of ATI

The intra-operator reliability of ATI was excellent with an ICC of 0.81 (95% CI: 0.71–0.88) and a CV of 9.4% (95% CI: 8.0–10.9). Intra-operator reliability of ATI was excellent with an ICC of 0.83 (95% CI: 0.51–0.94) and a CV of 7.3% (95% CI: 4.4–10.3) in patients with skin-to-liver distances <20 mm (n = 72) and an ICC of 0.78 (95% CI: 0.65–0.86) and a CV of 9.8% (95% CI: 8.1–11.5) in patients with skin-to-liver distances ≥20 mm (n = 15). The intra-operator reliability of ATI was excellent, with ICCs of 0.86 (95% CI: 0.73–0.92) and 0.89 (95% CI: 0.78–0.95) and CVs of 8.3% (95% CI: 6.4–10.3) and 7.3% (95% CI: 5.4–9.3) in patients with BMIs < 25 kg/m^2 (n = 47) and 25 ≤ BMI < 30 kg/m^2 (n = 33), respectively, whereas intra-operability of ATI was fair with an ICC of 0.56 (95% CI: −1.58 to 0.93) and a CV of 11.9% (95% CI: 4.0–20.5) in patients with BMI ≥ 30 kg/m^2 (n = 7).

DISCUSSION

We found that attenuation coefficients at ATI had a significant correlation with MRI-PDFF as well as excellent intra-operator reliability. Moreover, the attenuation

Table 2. Performance of ATI in the detection of hepatic steatosis

MRI-PDFF	Optimal cutoff of attenuation coefficients on ATI (dB/cm/MHz)	AUC (95% CI)	Sensitivity (%)	Specificity (%)
≥5%	0.59	0.76 (0.66–0.85)	88.0 (44/50)	62.2 (23/37)
≥10%	0.65	0.88 (0.79–0.94)	85.0 (17/20)	71.6 (48/67)

ATI = attenuation imaging; AUC = area under the receiver operating characteristic curve; CI = confidence interval; MRI-PDFF = magnetic resonance imaging proton-density fat fraction.

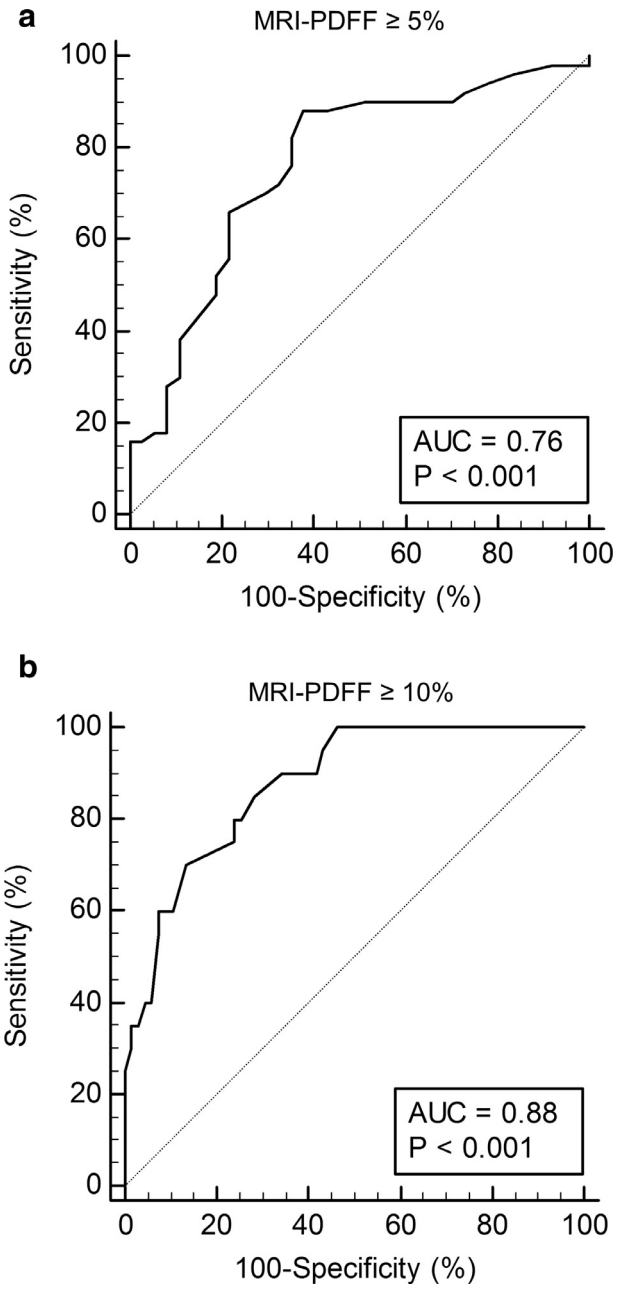

Fig. 3. Diagnostic accuracy of attenuation imaging for the (a) detection of hepatic steatosis defined by magnetic resonance imaging proton-density fat fraction (MRI-PDFF) ≥5% and (b) detection of hepatic fat content ≥10% defined as MRI-PDFF ≥10%. AUC = area under the curve.

coefficient at ATI was able to provide reasonably good diagnostic performance as a screening test for the detection of hepatic steatosis (MRI-PDFF ≥5%) and hepatic fat content ≥10% (MRI-PDFF ≥10%) (AUC: 0.76 and 0.88), respectively. In addition, although we did not directly compare the ATI and CAP with respect to diagnostic performance, the diagnostic accuracy of ATI in our study was comparable to the previously reported diagnostic performance of CAP for the detection of hepatic steatosis (AUC: 0.77−0.91) (Caussy et al. 2018; Chon et al. 2014; Karlas et al. 2017; Runge et al. 2018; Sasso et al. 2012; Shi et al. 2014). To date, MRI-PDFF measured by MR spectroscopy or multi-echo Dixon techniques has been proven to be the most accurate non-invasive quantitative modality for the assessment of hepatic steatosis, providing excellent correlation with histology-proven hepatic steatosis grades (Imajo et al. 2016; Noureddin et al. 2013; Runge et al. 2018). However, despite its high accuracy, MRI has a significantly higher cost than US-based techniques and limited availability, which has limited its adoption worldwide. In this regard, ultrasound-based techniques such as attenuation coefficient evaluation and acoustic structure quantification may represent alternative, easier options for the non-invasive assessment of hepatic steatosis (Fujiwara et al. 2018; Karlas et al. 2015; Lee et al. 2017b; Sasso et al. 2010; Son et al. 2016). To the best of our knowledge, this is the first prospective study to evaluate the diagnostic performance of ATI on a clinical US system in assessing hepatic steatosis using MRI-PDFF as the reference standard. Considering the high applicability and significant correlation of ATI with MRI-PDFF obtained in our study, ATI may be used as a first-line diagnostic tool for the assessment of hepatic steatosis.

The AUC of ATI for the detection of hepatic steatosis (MRI-PDFF ≥5%) was found to be 0.76 in our study patients. Compared with the results of previous studies using B-mode US-guided attenuation parameters in patients with NAFLD, however, the diagnostic accuracy of ATI in our study is slightly lower (Fujiwara et al. 2018; Lee et al. 2017b; Son et al. 2016). This may be due to differences in our study populations, as our study population comprised patients with various etiologies of CLDs, whereas previous studies included patients with only NAFLD or hepatitis C virus-related CLDs (Fujiwara et al. 2018; Son et al. 2016). Therefore, for the comparison of diagnostic accuracy between different ultrasound-based tools for hepatic steatosis staging, further studies with equivalent study populations (*e.g.,* patients with NAFLD) are warranted. We also investigated several factors that had the potential to affect ultrasound attenuation coefficients at ATI and determined that the degree of steatosis assessed at MRI-PDFF and the stage of fibrosis at MRE were significant determinant factors in the attenuation coefficient measured with ATI, which is in good agreement with the results of a previous study by Lee et al. (2017b). Moreover, we found that the correlation coefficient between ATI and MRI-PDFF was lower in patients with severe hepatic fibrosis than in those without severe fibrosis in our study. This may be because as speckles of the liver parenchyma change

Table 3. Factors affecting attenuation coefficients at attenuation imaging

Factor	Univariate analysis			Multivariate analysis		
	Coefficient	95% CI	*p* Value	Coefficient	95% CI	*p* Value
Male gender	−0.010	−0.057, 0.036	0.664			
Age	−0.001	−0.002, 0.002	0.822			
Type 2 diabetes	0.021	−0.032, 0.074	0.426			
Body mass index	0.011	0.005, 0.016	<0.001	0.003	−0.003, 0.009	0.274
Skin-to-capsular distance	0.009	0.005, 0.014	<0.001	0.002	−0.003, 0.007	0.371
Aspartate aminotransferase	0.001	−0.001, 0.002	0.418			
Alanine aminotransferase	0.002	0.001, 0.003	0.036	0.001	0.000, 0.002	0.069
Fibrosis stage	0.019	0.003, 0.036	0.024	0.017	0.006, 0.029	0.004
Liver stiffness at MRE	0.007	−0.004, 0.018	0.202			
MRI-PDFF	0.007	0.005, 0.009	<0.001	0.006	0.005, 0.008	<0.001

CI = confidence interval; MRE = magnetic resonance elastography; MRI-PDFF = magnetic resonance imaging proton-density fat fraction.

from homogeneous to heterogeneous during the progression of hepatic fibrosis (Toyoda et al. 2009), the presence of fibrosis may have also changed the US attenuation of the liver (Fujii et al. 2002; Lin et al. 1988). Therefore, in clinical application of ATI for the assessment of hepatic steatosis in patients with CLDs, the possibility of concurrent hepatic fibrosis should also be considered.

Liver fibrosis and steatosis are the two major features that need to be evaluated during assessment of the disease process or evaluation of treatment response in patients with NAFLD or steatogenic CLDs such as HCV infections and alcoholic liver disease (Park et al. 2017). Therefore, there is a clear clinical need to evaluate both liver fibrosis and steatosis quantitatively during longitudinal follow-up in the management of these patients (Angulo 2002; Berzigotti 2014; Elgouhari et al. 2009; Fabiani et al. 2018; Yu et al. 2017). In this regard, as both ATI and shear wave elastography can be made available on clinical scanners, the addition of 2-D shear wave elastography to ATI would be helpful in evaluating parenchymal damage in patients with CLDs and hepatic steatosis. Considering that several studies have already reported the reasonably good diagnostic performance of 2-D SWE in the staging of hepatic fibrosis (Lee et al. 2017c; Maruyama et al. 2016), further studies regarding the diagnostic performance of the combined use of ATI and shear wave elastography for the evaluation of hepatic fibrosis and steatosis in patients with CLDs are warranted.

Our study results also revealed the excellent intra-operator repeatability of ATI, which would be critical for the longitudinal evaluation of liver steatosis. Indeed, the repeatability of ATI was reported to be comparable to that of CAP (Ferraioli et al. 2014) and B-mode US-guided attenuation parameters reported in previous studies (Fujiwara et al. 2018; Son et al. 2016). Considering that ATI measurements are displayed in B-mode, whereas CAP is displayed in A-mode, ATI enables visual confirmation of the part to be measured with exclusion of structures that affect the measured values, such as vessels and extrahepatic areas (Fujiwara et al. 2018). In addition, ATI measurements and diagnostic gray-scale US evaluation can be performed concurrently in a single session, using a single probe and machine, which would be advantageous in clinical practice. However, a prospective head-to-head comparison between CAP and ATI using either MRI-PDFF or histologic assessment is warranted to determine the ideal screening test or the most optimal first-line diagnostic test for patients with NAFLD or CLD with steatosis.

There are some limitations to this study that need to be mentioned. First, histologic assessment of hepatic steatosis was not performed in this study. In its stead, we used MR-PDFF which is widely accepted as a reliable, novel standardized biomarker for the assessment of hepatic steatosis (Reeder et al. 2012). Indeed, according to several previous studies, MRI-PDFF has been proven to correlate well with magnetic resonance spectroscopy and histology-proven hepatic steatosis grades (Idilman et al. 2013; Le et al. 2012; Loomba et al. 2015; Permutt et al. 2012; Tang et al. 2013). Second, the etiology of liver diseases in our study population was heterogeneous. Third, inter-operator reproducibility could not be evaluated in this study, which may be important in the clinical application of ATI. Future studies are warranted in this regard. Fourth, there was a relatively long time delay between the two modalities. However, in subgroup analysis for the patients who underwent both ATI and MRI-PDFF on the same day, ATI had a correlation with MRI-PDFF similar to that for all study patients.

In conclusion, ATI was found to be well correlated with MRI-PDFF and thus may be a promising tool for the non-invasive assessment and quantification of hepatic steatosis that can provide good diagnostic performance.

Acknowledgments—This study was supported by a grant from Canon Medical Systems (No. 06-2017-3970)

APPENDIX A. IMAGING PARAMETERS FOR MRI-PDFF

Machine	TR (ms)	TE (ms)	ETL	Flip angle (°)	Slice thickness (mm)	Field of view (mm^2)	Matrix	Bandwidth (kHz)	Parallel imaging factor
Ingenia	6.1	0.95, 1.75, 2.55, 3.35, 4.15, 4.95	6	3	3	380 × 380	176 × 176	266	2
Skyra	9.3	1.05, 2.46, 3.69, 4.92, 6.15, 7.38	6	4	3	380 × 308	256 × 156	166	4
Discovery 750w	7.2	1.15, 2.3, 3.45, 4.6, 5.75, 6.9	3	3	10	380 × 380	320 × 256	100	2

MRI-PDFF = magnetic resonance imaging proton-density fat fraction

APPENDIX B. IMAGING PARAMETERS OF MRE

Magnetic resonance elastography was performed using a gradient echo sequence with the following imaging parameters: Repetition time and echo time = 50/20 ms; slice thickness = 6 mm; number of slices = 1; flip angle = 24; field of view = 30 × 35−40 × 45 cm^2; matrix = 256 × 80; one acquisition, number of excitations = 1, parallel imaging factor = 2, and one motion encoding gradient direction (craniocaudal) with four phase offsets. To obtain a consistent position of the liver for each phase offset, patients were instructed to hold their breath at the end of expiration. Four MRE slices were obtained for each patient. When acquisition was completed, wave images were automatically processed by the MR scanner, and images depicting tissue stiffness (elastograms) quantitatively (in kPa) were generated. In addition, the scanner software produced confidence maps to exclude areas of unreliable results caused by artifacts such as significant wave interference and oblique wave propagation, and elastograms with a 95% confidence threshold were produced.

REFERENCES

Angulo P. Nonalcoholic fatty liver disease. N Engl J Med 2002;346:1221–1231.

Berzigotti A. Getting closer to a point-of-care diagnostic assessment in patients with chronic liver disease: Controlled attenuation parameter for steatosis. J Hepatol 2014;60:910–912.

Blachier M, Leleu H, Peck-Radosavljevic M, Valla DC, Roudot-Thoraval F. The burden of liver disease in Europe: A review of available epidemiological data. J Hepatol 2013;58:593–608.

Caussy C, Alquiraish MH, Nguyen P, Hernandez C, Cepin S, Fortney LE, Ajmera V. Optimal threshold of controlled attenuation parameter with MRI-PDFF as the gold standard for the detection of hepatic steatosis. Hepatology 2018;67:1348–1359.

Chon YE, Jung KS, Kim SU, Park JY, Park YN, Kim DY, Ahn SH, Chon CY, Lee HW, Park Y, Han KH. Controlled attenuation parameter (CAP) for detection of hepatic steatosis in patients with chronic liver diseases: A prospective study of a native Korean population. Liver Int 2014;34:102–109.

Dasarathy S, Dasarathy J, Khiyami A, Joseph R, Lopez R, McCullough AJ. Validity of real time ultrasound in the diagnosis of hepatic steatosis: A prospective study. J Hepatol 2009;51:1061–1067.

Elgouhari HM, Zein CO, Hanouneh I, Feldstein AE, Zein NN. Diabetes mellitus is associated with impaired response to antiviral therapy in chronic hepatitis C infection. Dig Dis Sci 2009;54:2699–2705.

European Association for the Study of the Liver (EASL); European Association for the Study of Diabetes (EASD); European Association for the Study of Obesity (EASO). EASL−EASD−EASO Clinical Practice Guidelines for the management of non-alcoholic fatty liver disease. J Hepatol 2016;64(6):1388–1402.

Fabiani S, Fallahi P, Ferrari SM, Miccoli M, Antonelli A. Hepatitis C virus infection and development of type 2 diabetes mellitus: Systematic review and meta-analysis of the literature. Rev Endocr Metab Disord 2018;19:405–420.

Ferraioli G, Tinelli C, Lissandrin R, Zicchetti M, Rondanelli M, Perani G, Bernuzzi S, Salvaneschi L, Filice C. Interobserver reproducibility of the controlled attenuation parameter (CAP) for quantifying liver steatosis. Hepatol Int 2014;8:576–581.

Ferraioli G, Filice C, Castera L, Choi BI, Sporea I, Wilson SR, Cosgrove D, Dietrich CF, Amy D, Bamber JC, Barr R, Chou YH, Ding

H, Farrokh A, Friedrich-Rust M, Hall TJ, Nakashima K, Nightingale KR, Palmeri ML, Schafer F, Shiina T, Suzuki S, Kudo M. WFUMB guidelines and recommendations for clinical use of ultrasound elastography: Part 3. Liver. Ultrasound Med Biol 2015; 41:1161–1179.

Fujii Y, Taniguchi N, Itoh K, Shigeta K, Wang Y, Tsao JW, Kumasaki K, Itoh T. A new method for attenuation coefficient measurement in the liver: Comparison with the spectral shift central frequency method. J Ultrasound Med 2002;21:783–788.

Fujiwara Y, Kuroda H, Abe T, Ishida K, Oguri T, Noguchi S, Sugai T, Kamiyama N, Takikawa Y. The B-mode image-guided ultrasound attenuation parameter accurately detects hepatic steatosis in chronic liver disease. Ultrasound Med Biol 2018;44:2223–2232.

Hamaguchi M, Kojima T, Itoh Y, Harano Y, Fujii K, Nakajima T, Kato T, Takeda N, Okuda J, Ida K, Kawahito Y, Yoshikawa T, Okanoue T. The severity of ultrasonographic findings in nonalcoholic fatty liver disease reflects the metabolic syndrome and visceral fat accumulation. Am J Gastroenterol 2007;102:2708–2715.

Han A, Andre MP, Deiranieh L, Housman E, Erdman JW, Jr, Loomba R, Sirlin CB, O'Brien WD, Jr. Repeatability and reproducibility of the ultrasonic attenuation coefficient and backscatter coefficient measured in the right lobe of the liver in adults with known or suspected nonalcoholic fatty liver disease. J Ultrasound Med 2018; 27:1913–1927.

Huang SF, Chang IC, Hong CC, Yen TC, Chen CL, Wu CC, Tsai CC, Ho MC, Lee WC, Yu HC, Shen YY, Eng HL, Wang J, Tseng HH, Jeng YM, Yeh CT, Chen CL, Chen PJ, Liaw YF. Metabolic risk factors are associated with non-hepatitis B non-hepatitis C hepatocellular carcinoma in Taiwan, an endemic area of chronic hepatitis B. Hepatol Commun 2018;2:747–759.

Hudson JM, Milot L, Parry C, Williams R, Burns PN. Inter- and intra-operator reliability and repeatability of shear wave elastography in the liver: A study in healthy volunteers. Ultrasound Med Biol 2013; 39:950–955.

Idilman IS, Aniktar H, Idilman R, Kabacam G, Savas B, Elhan A, Celik A, Bahar K, Karcaaltincaba M. Hepatic steatosis: Quantification by proton density fat fraction with MR imaging versus liver biopsy. Radiology 2013;267:767–775.

Iellamo F, Legramante JM, Raimondi G, Castrucci F, Massaro M, Peruzzi G. Evaluation of reproducibility of spontaneous baroreflex sensitivity at rest and during laboratory tests. J Hypertens 1996; 14:1099–1104.

Imajo K, Kessoku T, Honda Y, Tomeno W, Ogawa Y, Mawatari H, Fujita K, Yoneda M, Taguri M, Hyogo H, Sumida Y, Ono M, Eguchi Y, Inoue T, Yamanaka T, Wada K, Saito S, Nakajima A. Magnetic resonance imaging more accurately classifies steatosis and fibrosis in patients with nonalcoholic fatty liver disease than transient elastography. Gastroenterology 2016;150:626–637.

Karlas T, Berger J, Garnov N, Lindner F, Busse H, Linder N, Schaudinn A, Relke B, Chakaroun R, Troltzsch M, Wiegand J, Keim V. Estimating steatosis and fibrosis: Comparison of acoustic structure quantification with established techniques. World J Gastroenterol 2015;21:4894–4902.

Karlas T, Petroff D, Sasso M, Fan JG, Mi YQ, de Ledinghen V, Kumar M, Lupsor-Platon M, Han KH, Cardoso AC, Ferraioli G, Chan WK, Wong VW, Myers RP, Chayama K, Friedrich-Rust M, Beaugrand M, Shen F, Hiriart JB, Sarin SK, Badea R, Jung KS, Marcellin P, Filice C, Mahadeva S, Wong GL, Crotty P, Masaki K, Bojunga J, Bedossa P, Keim V, Wiegand J. Individual patient data meta-analysis of controlled attenuation parameter (CAP) technology for assessing steatosis. J Hepatol 2017;66:1022–1030.

Le TA, Chen J, Changchien C, Peterson MR, Kono Y, Patton H, Cohen BL, Brenner D, Sirlin C, Loomba R. Effect of colesevelam on liver fat quantified by magnetic resonance in nonalcoholic steatohepatitis: A randomized controlled trial. Hepatology 2012;56:922–932.

Lee DH, Lee JM, Yi NJ, Lee KW, Suh KS, Lee JH, Lee KB, Han JK. Hepatic stiffness measurement by using MR elastography: Prognostic values after hepatic resection for hepatocellular carcinoma. Eur Radiol 2017a;27:1713–1721.

Lee DH, Lee JY, Lee KB, Han JK. Evaluation of hepatic steatosis by using acoustic structure quantification US in a rat model: Comparison with pathologic examination and mr spectroscopy. Radiology 2017b;285:445–453.

Lee ES, Lee JB, Park HR, Yoo J, Choi JI, Lee HW, Kim HJ, Choi BI, Park HJ, Park SB. Shear wave liver elastography with a propagation map: Diagnostic performance and inter-observer correlation for hepatic fibrosis in chronic hepatitis. Ultrasound Med Biol 2017c;43:1355–1363.

Lin T, Ophir J, Potter G. Correlation of ultrasonic attenuation with pathologic fat and fibrosis in liver disease. Ultrasound Med Biol 1988;14:729–734.

Loomba R, Sirlin CB, Ang B, Bettencourt R, Jain R, Salotti J, Soaft L, Hooker J, Kono Y, Bhatt A, Hernandez L, Nguyen P, Noureddin M, Haufe W, Hooker C, Yin M, Ehman R, Lin GY, Valasek MA, Brenner DA, Richards L. Ezetimibe for the treatment of nonalcoholic steatohepatitis: Assessment by novel magnetic resonance imaging and magnetic resonance elastography in a randomized trial (MOZART trial). Hepatology 2015;61:1239–1250.

Maruyama H, Kobayashi K, Kiyono S, Sekimoto T, Kanda T, Yokosuka O. Two-dimensional shear wave elastography with propagation-based reliability assessment for grading hepatic fibrosis and portal hypertension. J Hepatobiliary Pancreat Sci 2016; 23:595–602.

Mishra P, Younossi ZM. Abdominal ultrasound for diagnosis of nonalcoholic fatty liver disease (NAFLD). Am J Gastroenterol 2007;102:2716–2717.

Modaresi Esfeh J, Ansari-Gilani K. Steatosis and hepatitis C. Gastroenterol Rep (Oxf) 2016;4:24–29.

Noureddin M, Lam J, Peterson MR, Middleton M, Hamilton G, Le TA, Bettencourt R, Changchien C, Brenner DA, Sirlin C, Loomba R. Utility of magnetic resonance imaging versus histology for quantifying changes in liver fat in nonalcoholic fatty liver disease trials. Hepatology 2013;58:1930–1940.

Park CC, Nguyen P, Hernandez C, Bettencourt R, Ramirez K, Fortney L, Hooker J, Sy E, Savides MT, Alquiraish MH, Valasek MA, Rizo E, Richards L, Brenner D, Sirlin CB, Loomba R. Magnetic resonance elastography vs transient elastography in detection of fibrosis and noninvasive measurement of steatosis in patients with biopsy-proven nonalcoholic fatty liver disease. Gastroenterology 2017; 152:598–607 e2.

Permutt Z, Le TA, Peterson MR, Seki E, Brenner DA, Sirlin C, Loomba R. Correlation between liver histology and novel magnetic resonance imaging in adult patients with non-alcoholic fatty liver disease: MRI accurately quantifies hepatic steatosis in NAFLD. Aliment Pharmacol Ther 2012;36:22–29.

Reeder SB, Robson PM, Yu H, Shimakawa A, Hines CD, McKenzie CA, Brittain JH. Quantification of hepatic steatosis with MRI: The effects of accurate fat spectral modeling. J Magn Resonan Imaging 2009;29:1332–1339.

Reeder SB, Cruite I, Hamilton G, Sirlin CB. Quantitative assessment of liver fat with magnetic resonance imaging and spectroscopy. J Magn Reson Imaging 2011;34: spcone.

Reeder SB, Hu HH, Sirlin CB. Proton density fat-fraction: A standardized MR-based biomarker of tissue fat concentration. J Magn Reson Imaging 2012;36:1011–1014.

Rockey DC, Caldwell SH, Goodman ZD, Nelson RC, Smith AD. Liver biopsy. Hepatology 2009;49:1017–1044.

Runge JH, Smits LP, Verheij J, Depla A, Kuiken SD, Baak BC, Nederveen AJ, Beuers U, Stoker J. MR Spectroscopy-derived proton density fat fraction is superior to controlled attenuation parameter for detecting and grading hepatic steatosis. Radiology 2018;286:547–556.

Saadeh S, Younossi ZM, Remer EM, Gramlich T, Ong JP, Hurley M, Mullen KD, Cooper JN, Sheridan MJ. The utility of radiological imaging in nonalcoholic fatty liver disease. Gastroenterology 2002;123:745–750.

Sasso M, Beaugrand M, de Ledinghen V, Douvin C, Marcellin P, Poupon R, Sandrin L, Miette V. Controlled attenuation parameter (CAP): A novel VCTE guided ultrasonic attenuation measurement for the evaluation of hepatic steatosis: Preliminary study and validation in a cohort of patients with chronic liver disease from various causes. Ultrasound Med Biol 2010;36:1825–1835.

Sasso M, Miette V, Sandrin L, Beaugrand M. The controlled attenuation parameter (CAP)a novel tool for the non-invasive evaluation of steatosis using Fibroscan. Clin Res Hepatol Gastroenterol 2012;36:13–20.

Shi KQ, Tang JZ, Zhu XL, Ying L, Li DW, Gao J, Fang YX, Li GL, Song YJ, Deng ZJ, Wu JM, Tang KF. Controlled attenuation parameter for the detection of steatosis severity in chronic liver disease: A meta-analysis of diagnostic accuracy. J Gastroenterol Hepatol 2014;29:1149–1158.

Son JY, Lee JY, Yi NJ, Lee KW, Suh KS, Kim KG, Lee JM, Han JK, Choi BI. Hepatic steatosis: Assessment with acoustic structure quantification of US imaging. Radiology 2016;278:257–264.

Tang A, Tan J, Sun M, Hamilton G, Bydder M, Wolfson T, Gamst AC, Middleton M, Brunt EM, Loomba R, Lavine JE, Schwimmer JB, Sirlin CB. Nonalcoholic fatty liver disease: MR imaging of liver proton density fat fraction to assess hepatic steatosis. Radiology 2013;267:422–431.

Toyoda H, Kumada T, Kamiyama N, Shiraki K, Takase K, Yamaguchi T, Hachiya H. B-Mode ultrasound with algorithm based on statistical analysis of signals: Evaluation of liver fibrosis in patients with chronic hepatitis C. AJR Am J Roentgenol 2009;193:1037–1043.

Xiao H, Shi M, Xie Y, Chi X. Comparison of diagnostic accuracy of magnetic resonance elastography and Fibroscan for detecting liver fibrosis in chronic hepatitis B patients: A systematic review and meta-analysis. 2017;12:e0186660.

Yokoo T, Serai SD, Pirasteh A, Bashir MR, Hamilton G, Hernando D, Hu HH, Hetterich H, Kuhn JP, Kukuk GM, Loomba R, Middleton MS, Obuchowski NA, Song JS, Tang A, Wu X, Reeder SB, Sirlin CB. for the RSNA-QIBA PDFF Biomarker Committee. Linearity, bias, and precision of hepatic proton density fat fraction measurements by using MR imaging: A meta-analysis. Radiology 2018;286:486–498.

Yoon JH, Lee JM, Woo HS, Yu MH, Joo I, Lee ES, Sohn JY, Lee KB, Han JK, Choi BI. Staging of hepatic fibrosis: Comparison of magnetic resonance elastography and shear wave elastography in the same individuals. Korean J Radiol 2013;14:202–212.

Youden WJ. Index for rating diagnostic tests. Cancer 1950;3:32–35.

Yu MW, Lin CL, Liu CJ, Yang SH, Tseng YL, Wu CF. Influence of metabolic risk factors on risk of hepatocellular carcinoma and liver-related death in men with chronic hepatitis B: A large cohort study. Gastroenterology 2017;153:1006–1017 e5.